THE JOURNAL OF PHYSICAL CHEMISTRY B

Article

Cite This: J. Phys. Chem. B 2019, 123, 787−791

pubs.acs.org/JPCB

Bacteriostatic Effects of Apatite-Covered Ag/AgBr/TiO_2 Nanocomposite in the Dark: Anomaly in Bacterial Motility

Seyedsaeid Ahmadvand,*[,†] Mohammadreza Elahifard,[‖] Mehdi Jabbarzadeh,[⊥] Amir Mirzanejad,[‖] Kathryn Pflughoeft,[‡] Bahman Abbasi,[#] and Behrooz Abbasi[§]

[†]Department of Chemistry, [‡]School of Medicine, Department of Microbiology and Immunology, and [§]Department of Metallurgical Engineering, University of Nevada, Reno, Reno, Nevada 89557, United States

[‖]Chemical Engineering Department, Faculty of Engineering, Ardakan University, Ardakan 89518-95491, Iran

[⊥]Department of Mechanical Engineering, University of Utah, Salt Lake City, Utah 84112, United States

[#]Department of Mechanical Engineering, Oregon State University, Corvallis, Oregon 97333, United States

Supporting Information

ABSTRACT: In this paper, we report a unique property of inactivating Gram-positive/negative bacteria in the dark via apatite-covered Ag/AgBr/TiO_2 nanocomposites (AAAT). We demonstrate that the inactivation mechanism is bacteriostatic based on the cellular integrity and motility of bacteria, low toxicity and high durability of AAAT. From straight observations, the catalytic loading affects the bacterial replication and cell envelope as well as inducing an anomaly in bacterial motility (continuous rotation) for both types of bacteria. Both simulation and experimental analyses suggest that the anomaly could be due to posterior intracellular signals rather than purely mechanical effects (e.g., size enlargement and motility retardation). Provoked by chemomechanical stimuli, these signals increase the frequency of flagellar tumbling and eventually entangle the bacteria.

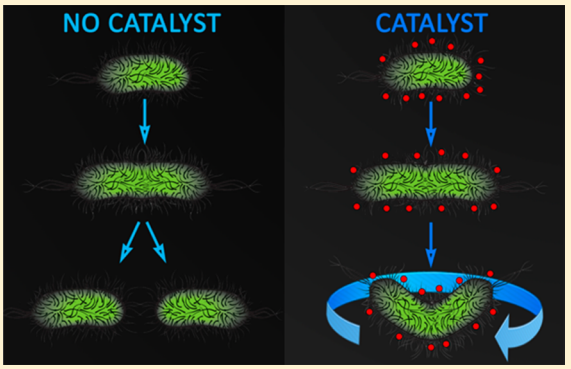

1. INTRODUCTION

Most antibiotics are bactericidal and inactivate bacteria via lysis (e.g., penicillin).[1−4] Apart from lysis, chemicals can inactivate bacteria by changing the cellular biochemistry, motility, and reproduction.[5−8] When a bacterial cell encounters a chemoattractant or a repellent that binds to a chemoreceptor, a ligand-induced conformational change may occur in the chemoreceptor.[9−12] The downstream effect is a change in the ratio of the concentration of phosphorylated to unphosphorylated forms of the CheY protein and thereby flagellar motion.[13,14] Bacteria tumble less frequently facing an attractant and more frequently facing a repellent, governed by the concentration of phosphorylated CheY.[13−18] Other stimuli can also disrupt bacterial motility, such as catalytic loading of bacteria.[8]

The scope of action, toxicity, and durability are three major concerns in the synthesis of bacteriostatic materials.[19−26] Numerous studies have reported bacteriostatic effects of materials, in which silver, titanium, and phosphate components are individually and combinatorially present.[27−31] These effects become more prominent when all aforementioned compounds exist simultaneously.[32−35] For instance, a bacteriostatic activity has been reported for the porous material, $AgTi_2(PO_4)_3$, with a very small out-leaching of Ag^+ ion (<10 μequiv g^{-1}).[36] At low concentrations of silver ions, the synthesis of a porous sandwich nanostructure of titanate/silver/titanate with a bacteriostatic rate of 99% has been reported.[37] The degree of bacteriostatic activity of these porous material has been attributed to an engineered out-leaching of Ag^+ ions in the environment but not direct contact of the integrated silver element.[38] Silver ions are well known as bactericidal agents, but they have also exhibited bacteriostatic effects at low concentrations, such as inhibition of cell reproduction.[39]

Photocatalytic bactericidicity of TiO_2 and its derivatives have been widely studied in different regions of the electromagnetic spectrum.[30,40−44] Apatite and Ag/AgBr are introduced to TiO_2 photocatalytic family as adsorbent and photosensitive agents, respectively.[45−47] The antibacterial properties of AAAT are modified compared to those of TiO_2, Ag/AgBr/TiO_2, and apatite-covered TiO_2 in the presence of light.[41,47] In the absence of light, however, the antibacterial functionality of AAAT is yet unresolved. The hydrogen bond between the phosphate group of AAAT and bacteria extracellular polysaccharides has been suggested as the origin of the strong adherence between the two. This adherence has been proposed to obstruct the bacterial outer membrane of *Escherichia coli* and thus nutrition, while not decomposing the cell wall.[46] This proposal raises few

Received: November 2, 2018
Revised: January 7, 2019
Published: January 8, 2019

DOI: 10.1021/acs.jpcb.8b10710
J. Phys. Chem. B 2019, 123, 787−791

unanswered questions: (1) If the phosphate group is responsible for the adherence on the catalyst end, why is apatite-covered TiO_2 ineffective? (2) What are the possible chemical effects of this adherence? (3) If the cell wall is not damaged, does the catalytic loading of bacteria trigger the inactivation process? (4) Do (chemo)mechanical stimuli influence the bacterial motility and how would this affect the inactivation of bacteria? Herein, we seek possible answers to these questions to provide a better understanding of the nature of the inactivation mechanism.

2. MATERIALS AND METHODS

Apatite-coated $Ag/AgBr/TiO_2$ was prepared as a sample of synthesized antibacterial group, through deposition of hydroxyapatite, as adsorption bioceramic, and AgBr, as photosensitive material. The preparation procedure has been explained elsewhere (ref 46 of the paper). To measure the catalytic activity under dark media, 24 mg of photocatalyst was added to bacterial suspension. The *E. coli* (ATCC, 8739) and *Bacillus subtilis* (ATCC, 6633) were prepared in 1×10^7 colony-forming units (CFU mL^{-1}) bacterial cell concentration. The reaction mixture was stirred with a magnetic stirrer to prevent the precipitation of the photocatalysts, and in certain time intervals, 2 mL of the reaction mixture was diluted with 0.9% saline. Then, 1 mL of diluted solution was incubated at 37 °C for 24 h on soybean casein digest agar, and the colonies were counted. For the transmission electron microscopy (TEM) analysis, the samples were prepared according to the standard procedure. A photocamera coupled with optical microscope was used to follow the motion of bacteria.

3. RESULTS AND DISCUSSION

3.1. Experiment. AAAT exhibits similar inactivation rates for both Gram-negative and Gram-positive bacteria, organisms with different cell envelope structures, in the dark (Figure 1).

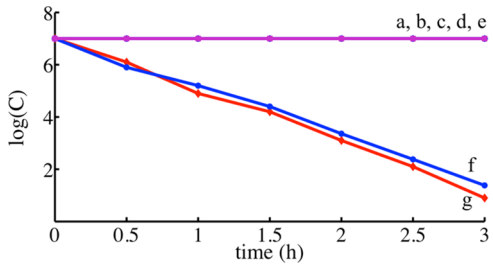

Figure 1. Temporal course of the *E. coli* and *B. subtilis* inactivation (1×10^7, 30 mL) in aqueous dispersions containing 24 mg of catalysts: (a) apatite, (b) Ag/TiO_2, (c) $Ag/AgBr/TiO_2$, (d) apatite-covered TiO_2, (e) TiO_2/P-2, (f) AAAT (acting on *B. subtilis*), and (g) AAAT (acting on *E. coli*) in the dark. Catalysts (a)−(e) are inactive on both bacteria types.

Atomic absorbance spectroscopy shows an insignificant increase in the concentration of antibacterial silver ions in the environment (Figure S1). In addition, the increment of CO_2, a byproduct of oxo-degradation, is insignificant in the dark (Figure S2). Finally, the uncompromised integrity of the cell envelope suggests that the undefined mechanism of inactivation by AAAT has nonlytic nature (Figures 2 and 3). All aforementioned evidences suggest that the cell envelope is not chemically decomposed, and bacterial inactivation may have bacteriostatic origins. Monitoring the bacterial motility under the exposure to AAAT (up to 3 h) confirms that both *E. coli* and *B. subtilis* retain mobility, yet cease replication (Movies S1 and S2). Therefore, we propose that AAAT is bacteriostatic rather than bactericidal in the absence of light, contrary to the presence of light.

From the chemical point of view, inefficiency of apatite alone (source of phosphate) and apatite-covered TiO_2 raises doubts about phosphate groups being the only responsible for bacteriostaticity of AAAT (Figure 1). In addition, the neutrality of $Ag/AgBr/TiO_2$ and TiO_2 suggests that all components participate in the bacteriostatic efficiency of AAAT. Neutral catalysts in Figure 1a−e remain inactive, even at higher dosages (up to 48 mg). Energy-dispersive X-ray analysis indicates that mainly phosphate and Ti (as in TiO_2) interact with the bacterial surface (Table S1). Compared to other apatite containing catalysts, the bacteriostaticity of AAAT can be attributed to its higher (∼10 to 15%) Brunauer−Emmett−Teller[48] surface (48 m^2 g^{-1}). This can increase the AAAT−bacterium interface and maintain the out-leaching of silver ions at a proper level for bacteriostatic purposes. However, $Ag/AgBr/TiO_2$ releases similar amount of silver ions (<1%) in the solution and yet unable to inactivate bacteria within the scope of the experiment. Further assessment on the physicochemical properties of AAAT is in progress to perceive more on its significant bacteriostaticity and adsorbability against bacteria. A rough estimate of bacterial growth implies that cell replication proceeds up to elongation step prior to arrest (Figure S4). Also, the oscillation in pH of the AAAT/bacteria solution (7.0−7.3), whereas pH of the AAAT bare solution is about 7.5, could be an indicator of disruption of the cellular net proton transfer.[31] Taken together, we speculate that the bacteriostatic mechanism relies on not only direct consequences of the AAAT−bacterium bond (e.g., cell obstruction) but also posterior chemical effects (e.g., endogenous imbalance).

3.2. Simulation. Mechanically speaking, the bacteriostatic mechanism could be explained by an anomaly in the motility of bacteria that is induced by the AAAT surficial fixation. As Figure 3 shows, the heterogeneous AAAT−bacterium adherence makes the bacterium heavier and less flexible, therefore, few flagella may fly apart, and the average forward run velocity drops. This emerges as a random run and tumble motility with a preferable rotation around the more flexible (less loaded) side and intermittent stops (Figure 4). In most cases, a constant tumbling motion is observed without any sensible forward motion (Movies S1 and S2). This leads to a unique rotational motion that is different from the circular trajectory near the solid boundaries and glass surfaces due to the following reasons: (1) the rotational motion occurs in an almost fixed position, (2) tumbling motion dynamically converts clockwise (CW) and counterclockwise (CCW) motions to each other, (3) the frequency of the rotational motion is about 1 order of magnitude (∼1 Hz) smaller than that of the circular trajectory (10 Hz).[49,50] The mechanical origin of this motion is the catalytic loading of bacteria such that the forward motion is hindered. As a result, the average forward run velocity changes as a function of size growth and uniformity (Figures S7 and S8). Even for extreme cases (e.g., 50× growth), the average run velocity is significant; nearly 35 and 15 $\mu m\ s^{-1}$ for run and tumble and conventional tumble (0.1 time scale) motilities, respectively. The increment of tumbling frequency, however, reduces the average run velocity further, independent of the bacterial size and uniformity

DOI: 10.1021/acs.jpcb.8b10710
J. Phys. Chem. B 2019, 123, 787−791

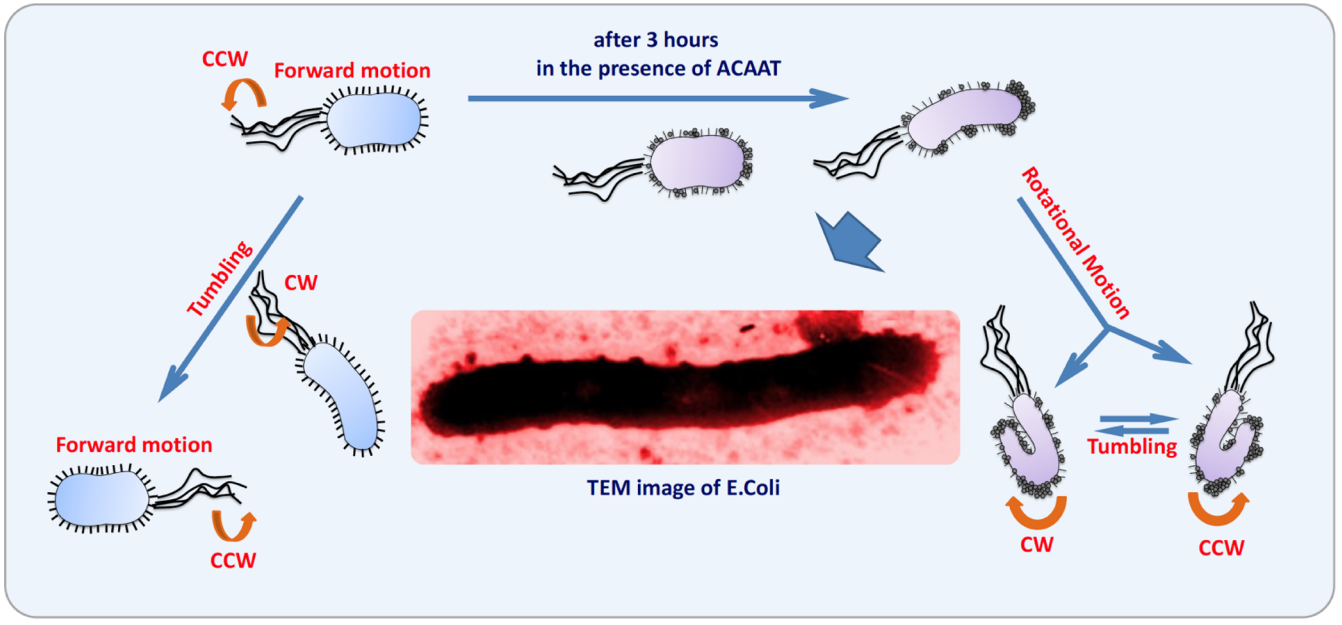

Figure 2. Schematic representation of rotational motion of *E. coli* under the influence of the AAAT. The TEM image indicates that the cell wall is undamaged (the interior remains dark). Clockwise (CW) and counterclockwise (CCW) refer to the flagellar motion on the left side and cellular motion on the right side, respectively.

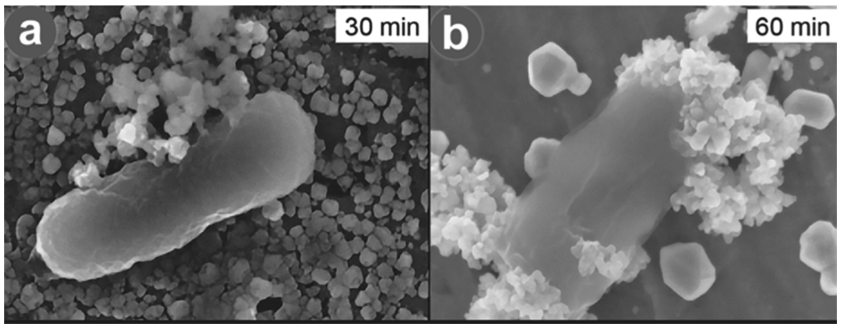

Figure 3. Scanning electron microscopy images of the heterogeneous adherence of AAAT to the surface of *E. coli* at two different time intervals: (a) after 30 min, (b) after 60 min, in the dark (scale bar = 100 nm).

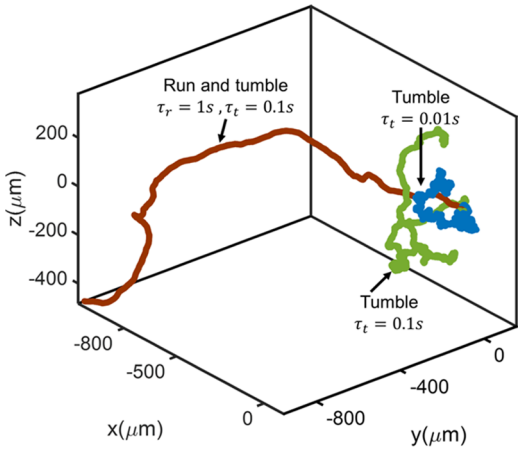

Figure 4. Mechanically modeled trajectories of the run and tumble (red), conventional tumble (green), and high-frequency tumble (blue) motilities of *E. coli* bacterium.

(Figure S8b). The trajectory of such motility (Figure 4) provides a better explanation for the observed rotational motion. A higher frequency tumbling could reduce the mismatch between simulation and experiment, provoked by endogenous/induced chemotactic signals.

4. CONCLUSIONS

The evaluation of the cell integrity, matrix toxicity, inactivation rate, and bacterial motility demonstrate a bacteriostatic inactivation of *E. coli* and *B. subtilis* bacteria when AAAT is introduced in the dark. Similar to previous studies, structural analyses suggest that bacteriostaticity is interconnected to the porosity of AAAT and its strong adherence to the bacterial surface. We speculate that TiO_2, Ag/AgBr, and apatite serve as the matrix, poring, and adsorbent agents in the structure of AAAT, respectively. The hydroxyl group (as in apatite) could also participate in the reduction of silver ions, cellular proton transfer, and porosity of the nanocomposite.[36] A purely mechanical effect of catalytic loading is expected to be a retardation of the bacterial motility as a result of its enlargement, evidenced in both simulation and experiment. Nevertheless, modeling this effect fails to capture a quantitative/qualitative feature of the observed rotational motion. On the other hand, increasing the tumbling frequency, induced by intracellular/extracellular stimuli, can better capture this feature. Overall, this study elucidates a few

DOI: 10.1021/acs.jpcb.8b10710
J. Phys. Chem. B 2019, 123, 787−791

chemomechanical origins of the AAAT-induced inactivation of bacteria but leaves many questions unanswered. Among nanomaterials, those with silver, titanium, and phosphate in common have exhibited similar properties such as high durability (slow out-leaching of Ag^+), bacteriostaticity, and porosity, and low toxicity. We strongly suggest that a new class of nanomaterials, in which those properties are modified, is potentially applicable for the in vivo studies and drug delivery.

■ ASSOCIATED CONTENT

Supporting Information

The Supporting Information is available free of charge on the ACS Publications website at DOI: 10.1021/acs.jpcb.8b10710.

ACAAT synthesis and characterization, mechanical modeling (PDF)

After 3 h exposure to AAAT catalyst motion of *E. coli* in the dark (AVI)

After 3 h exposure to AAAT catalyst motion of *B. subtilis* in the dark (AVI)

■ AUTHOR INFORMATION

Corresponding Author

*E-mail: sahmadvand@unr.edu. Tel: 775-771-4765.

ORCID

Seyedsaeid Ahmadvand: 0000-0001-7888-262X

Author Contributions

The manuscript is written through equal contributions of all authors.

Notes

The authors declare no competing financial interest.

■ ACKNOWLEDGMENTS

We are grateful to University of Nevada, Reno, for financial support in the form of the start-up fund for B.A. This work was supported by two DOE and ARPA-E Awards (DE-FOA-0001778 and DE-FOA-0001858). We thank A. O. Lykhin for valuable suggestions.

■ REFERENCES

(1) Meeske, A. J.; Riley, E. P.; Robins, W. P.; Uehara, T.; Mekalanos, J. J.; Kahne, D.; Walker, S.; Kruse, A. C.; Bernhardt, T. G.; Rudner, D. Z. SEDS Proteins Are a Widespread Family of Bacterial Cell Wall Polymerases. *Nature* **2016**, *537*, 634−638.

(2) Typas, A.; Banzhaf, M.; van den Berg van Saparoea, B.; Verheul, J.; Biboy, J.; Nichols, R. J.; Zietek, M.; Beilharz, K.; Kannenberg, K.; von Rechenberg, M.; et al. Regulation of Peptidoglycan Synthesis by Outer-Membrane Proteins. *Cell* **2010**, *143*, 1097−1109.

(3) Johnson, D. S.; Weerapana, E.; Cravatt, B. F. Strategies for Discovering and Derisking Covalent, Irreversible Enzyme Inhibitors. *Future Med. Chem.* **2010**, *2*, 949−964.

(4) Silhavy, T. J.; Kahne, D.; Walker, S. The Bacterial Cell Envelope. *Cold Spring Harbor Perspect. Biol.* **2010**, *2*, No. a000414.

(5) Deng, X.; Liang, H.; Ulanovskaya, O. A.; Ji, Q.; Zhou, T.; Sun, F.; Lu, Z.; Hutchison, A. L.; Lan, L.; Wu, M.; et al. Steady-State Hydrogen Peroxide Induces Glycolysis in *Staphylococcus aureus* and *Pseudomonas aeruginosa*. *J. Bacteriol.* **2014**, *196*, 2499−2513.

(6) Balakrishnan, A.; Patel, B.; Sieber, S. A.; Chen, D.; Pachikara, N.; Zhong, G.; Cravatt, B. F.; Fan, H. Metalloprotease Inhibitors GM6001 and TAPI-0 Inhibit the Obligate Intracellular Human Pathogen *Chlamydia trachomatis* by Targeting Peptide Deformylase of the Bacterium. *J. Biol. Chem.* **2006**, *281*, 16691−16699.

(7) Kim, T.; Hyeon, T. Applications of Inorganic Nanoparticles as Therapeutic Agents. *Nanotechnology* **2014**, *25*, No. 012001.

(8) Syal, K.; Iriya, R.; Yang, Y.; Yu, H.; Wang, S.; Haydel, S. E.; Chen, H.-Y.; Tao, N. Antimicrobial Susceptibility Test with Plasmonic Imaging and Tracking of Single Bacterial Motions on Nanometer Scale. *ACS Nano* **2016**, *10*, 845−852.

(9) Sharff, A. J.; Rodseth, L. E.; Spurlino, J. C.; Quiocho, F. A. Crystallographic Evidence of a Large Ligand-Induced Hinge-Twist Motion between the Two Domains of the Maltodextrin Binding Protein Involved in Active Transport and Chemotaxis. *Biochemistry* **1992**, *31*, 10657−10663.

(10) Murphy, O. J.; Kovacs, F. A.; Sicard, E. L.; Thompson, L. K. Site-Directed Solid-State NMR Measurement of a Ligand-Induced Conformational Change in the Serine Bacterial Chemoreceptor. *Biochemistry* **2001**, *40*, 1358−1366.

(11) Gestwicki, J. E.; Hsieh, H. V.; Pitner, J. B. Using Receptor Conformational Change to Detect Low Molecular Weight Analytes by Surface Plasmon Resonance. *Anal. Chem.* **2001**, *73*, 5732−5737.

(12) Jeffrey, P. D.; Bewley, M. C.; MacGillivray, R. T. A.; Mason, A. B.; Woodworth, R. C.; Baker, E. N. Ligand-Induced Conformational Change in Transferrins: Crystal Structure of the Open Form of the N-Terminal Half-Molecule of Human Transferrin. *Biochemistry* **1998**, *37*, 13978−13986.

(13) Kakuda, T.; DiRita, V. J. Cj1496c Encodes a *Campylobacter jejuni* Glycoprotein That Influences Invasion of Human Epithelial Cells and Colonization of the Chick Gastrointestinal Tract. *Infect. Immun.* **2006**, *74*, 4715−4723.

(14) Rao, C. V.; Kirby, J. R.; Arkin, A. P. Design and Diversity in Bacterial Chemotaxis: A Comparative Study in *Escherichia coli* and *Bacillus subtilis*. *PLoS Biol.* **2004**, *2*, No. e49.

(15) Wang, W.; Duan, W.; Ahmed, S.; Sen, A.; Mallouk, T. E. From One to Many: Dynamic Assembly and Collective Behavior of Self-Propelled Colloidal Motors. *Acc. Chem. Res.* **2015**, *48*, 1938−1946.

(16) Mallouk, T. E.; Sen, A. Powering Nanorobots. *Sci. Am.* **2009**, *300*, 72−77.

(17) Dey, K. K.; Das, S.; Poyton, M. F.; Sengupta, S.; Butler, P. J.; Cremer, P. S.; Sen, A. Chemotactic Separation of Enzymes. *ACS Nano* **2014**, *8*, 11941−11949.

(18) Mao, H.; Cremer, P. S.; Manson, M. D. A Sensitive, Versatile Microfluidic Assay for Bacterial Chemotaxis. *Proc. Natl. Acad. Sci.* **2003**, *100*, 5449−5454.

(19) Mukhtar, T. A.; Wright, G. D.; Streptogramins. Oxazolidinones, and Other Inhibitors of Bacterial Protein Synthesis. *Chem. Rev.* **2005**, *105*, 529−542.

(20) Yuan, T.; Sampson, N. S. Hit Generation in TB Drug Discovery: From Genome to Granuloma. *Chem. Rev.* **2018**, *118*, 1887−1916.

(21) Li, J.; Liu, X.; Qiao, Y.; Zhu, H.; Li, J.; Cui, T.; Ding, C. Enhanced Bioactivity and Bacteriostasis Effect of TiO_2 Nanofilms with Favorable Biomimetic Architectures on Titanium Surface. *RSC Adv.* **2013**, *3*, 11214.

(22) Carson, J. F.; Jansen, E. F.; Lewis, J. C. Esterification of Subtilin and Its Effect on Solubility and in Vitro Bacteriostatic Activity. *J. Am. Chem. Soc.* **1949**, *71*, 2318−2322.

(23) Kumler, W. D.; Daniels, T. C. The Relation Between Chemical Structure and Bacteriostatic Activity of Sulfanilamide Type Compounds. *J. Am. Chem. Soc.* **1943**, *65*, 2190−2196.

(24) Beaver, D. J.; Roman, D. P.; Stoffel, P. J. The Preparation and Bacteriostatic Activity of Substituted Ureas. *J. Am. Chem. Soc.* **1957**, *79*, 1236−1245.

(25) Beaver, D. J.; Shumard, R. S.; Stoffel, P. J. Preparation and Bacteriostatic Properties of Substituted Trisphenols. *J. Am. Chem. Soc.* **1953**, *75*, 5579−5581.

(26) Silva, L. N.; Zimmer, K. R.; Macedo, A. J.; Trentin, D. S. Plant Natural Products Targeting Bacterial Virulence Factors. *Chem. Rev.* **2016**, *116*, 9162−9236.

(27) Stelzig, S. H.; Menneking, C.; Hoffmann, M. S.; Eisele, K.; Barcikowski, S.; Klapper, M.; Müllen, K. Compatibilization of Laser Generated Antibacterial Ag- and Cu-Nanoparticles for Perfluorinated Implant Materials. *Eur. Polym. J.* **2011**, *47*, 662−667.

DOI: 10.1021/acs.jpcb.8b10710
J. Phys. Chem. B 2019, 123, 787−791

(28) Hosono, H.; Tsuchitani, F.; Imai, K.; Abe, Y.; Maeda, M. Porous Glass-Ceramics Cation Exchangers: Cation Exchange Properties of Porous Glass-Ceramics with Skeleton of Fast Li Ion-Conducting $LiTi_2(PO_4)_3$ Crystal. *J. Mater. Res.* **1994**, *9*, 755−761.
(29) Hoyos-Nogués, M.; Buxadera-Palomero, J.; Ginebra, M.-P.; Manero, J. M.; Gil, F.; Mas-Moruno, C. All-in-One Trifunctional Strategy: A Cell Adhesive, Bacteriostatic and Bactericidal Coating for Titanium Implants. *Colloids Surf., B* **2018**, *169*, 30−40.
(30) Li, J.; Liu, X.; Qiao, Y.; Zhu, H.; Ding, C. Antimicrobial Activity and Cytocompatibility of Ag Plasma-Modified Hierarchical TiO_2 Film on Titanium Surface. *Colloids Surf., B* **2014**, *113*, 134−145.
(31) Cao, H.; Liu, X.; Meng, F.; Chu, P. K. Biological Actions of Silver Nanoparticles Embedded in Titanium Controlled by Micro-Galvanic Effects. *Biomaterials* **2011**, *32*, 693−705.
(32) Kasuga, T.; Kume, H.; Abe, Y. Porous Glass-Ceramics with Bacteriostatic Properties in Silver-Containing Titanium Phosphates: Control of Release of Silver Ions from Glass-Ceramics into Aqueous Solution. *J. Am. Ceram. Soc.* **1997**, *80*, 777−780.
(33) Kasuga, T.; Nogami, M.; Abe, Y. Titanium Phosphate Glass-Ceramics with Silver Ion Exchangeability. *J. Am. Ceram. Soc.* **2004**, *82*, 765−767.
(34) Kasuga, T.; Kume, H.; Nogami, M.; Abe, Y.; Hosono, H. Porous Titanium Phosphate Glass-Ceramics with Bacteriostatic Activities. *Phosphorus Res. Bull.* **1996**, *6*, 253−256.
(35) Hosono, H.; Abe, Y. Silver Ion Selective Porous Lithium Titanium Phosphate Glass-Ceramics Cation Exchanger and Its Application to Bacteriostatic Materials. *Mater. Res. Bull.* **1994**, *29*, 1157−1162.
(36) Kasuga, T.; Nakamura, H.; Yamamoto, K.; Nogami, M.; Abe, Y. Microporous Materials with an Integrated Skeleton of $AgTi_2(PO_4)_3$ and $Ti(HPO_4)_2{\cdot}2H_2O$ Crystals. *Chem. Mater.* **1998**, *10*, 3562−3567.
(37) Ren, N.; Li, R.; Chen, L.; Wang, G.; Liu, D.; Wang, Y.; Zheng, L.; Tang, W.; Yu, X.; Jiang, H.; et al. In Situ Construction of a Titanate−Silver Nanoparticle−Titanate Sandwich Nanostructure on a Metallic Titanium Surface for Bacteriostatic and Biocompatible Implants. *J. Mater. Chem.* **2012**, *22*, 19151.
(38) Thiel, J.; Pakstis, L.; Buzby, S.; Raffi, M.; Ni, C.; Pochan, D. J.; Shah, S. I. Antibacterial Properties of Silver-Doped Titania. *Small* **2007**, *3*, 799−803.
(39) Navarro, E.; Piccapietra, F.; Wagner, B.; Marconi, F.; Kaegi, R.; Odzak, N.; Sigg, L.; Behra, R. Toxicity of Silver Nanoparticles to *Chlamydomonas reinhardtii*. *Environ. Sci. Technol.* **2008**, *42*, 8959−8964.
(40) Elahifard, M. R.; Ahmadvand, S.; Mirzanejad, A. Effects of Ni-Doping on the Photo-Catalytic Activity of TiO_2 Anatase and Rutile: Simulation and Experiment. *Mater. Sci. Semicond. Process.* **2018**, *84*, 10−16.
(41) Elahifard, M. R.; Rahimnejad, S.; Pourbaba, R.; Haghighi, S.; Gholami, M. R. Photocatalytic Mechanism of Action of Apatite-Coated $Ag/AgBr/TiO_2$ on Phenol and *Escherichia coli* and *Bacillus subtilis* Bacteria under Various Conditions. *Prog. React. Kinet. Mech.* **2011**, *36*, 38−52.
(42) Chen, S.; Guo, Y.; Zhong, H.; Chen, S.; Li, J.; Ge, Z.; Tang, J. Synergistic Antibacterial Mechanism and Coating Application of Copper/Titanium Dioxide Nanoparticles. *Chem. Eng. J.* **2014**, *256*, 238−246.
(43) Akimov, A. V.; Prezhdo, O. V. Large-Scale Computations in Chemistry: A Bird's Eye View of a Vibrant Field. *Chem. Rev.* **2015**, *115*, 5797−5890.
(44) Pérez-Anes, A.; Gargouri, M.; Laure, W.; Van Den Berghe, H.; Courcot, E.; Sobocinski, J.; Tabary, N.; Chai, F.; Blach, J.-F.; Addad, A.; et al. Bioinspired Titanium Drug Eluting Platforms Based on a Poly-β-Cyclodextrin−Chitosan Layer-by-Layer Self-Assembly Targeting Infections. *ACS Appl. Mater. Interfaces* **2015**, *7*, 12882−12893.
(45) Hu, C.; Lan, Y.; Qu, J.; Hu, X.; Wang, A. $Ag/AgBr/TiO_2$ Visible Light Photocatalyst for Destruction of Azodyes and Bacteria. *J. Phys. Chem. B* **2006**, *110*, 4066−4072.
(46) Elahifard, M. R.; Rahimnejad, S.; Haghighi, S.; Gholami, M. R. Apatite-Coated $Ag/AgBr/TiO_2$ Visible-Light Photocatalyst for Destruction of Bacteria. *J. Am. Chem. Soc.* **2007**, *129*, 9552−9553.
(47) Nonami, T.; Hase, H.; Funakoshi, K. Apatite-Coated Titanium Dioxide Photocatalyst for Air Purification. *Catal. Today* **2004**, *96*, 113−118.
(48) Brunauer, S.; Emmett, P. H.; Teller, E. Adsorption of Gases in Multimolecular Layers. *J. Am. Chem. Soc.* **1938**, *60*, 309−319.
(49) Berg, H. C.; Turner, L. Chemotaxis of Bacteria in Glass Capillary Arrays. *Escherichia coli*, Motility, Microchannel Plate, and Light Scattering. *Biophys. J.* **1990**, *58*, 919−930.
(50) Miño, G.; Mallouk, T. E.; Darnige, T.; Hoyos, M.; Dauchet, J.; Dunstan, J.; Soto, R.; Wang, Y.; Rousselet, A.; Clement, E. Enhanced Diffusion Due to Active Swimmers at a Solid Surface. *Phys. Rev. Lett.* **2011**, *106*, No. 048102.

DOI: 10.1021/acs.jpcb.8b10710
J. Phys. Chem. B 2019, 123, 787−791